Modulations in relaxor nature due to Sr^{2+} doping in 0.68PMN-0.32PT ceramic

Pius Augustine[a,b,c,*], Muralidhar Miryala[c], Shibnath Samanta[d], S. Pavan Kumar Naik[c], K. Sethupathi[d], Masato Murakami[c], M.S. Ramachandra Rao[b,**]

[a] Department of Physics, Sacred Heart College (Autonomous), Kochi, 682013, India
[b] Department of Physics, Nano Functional Material Technology Centre and Material Science Research Centre, Indian Institute of Technology Madras, Chennai, 600036, India
[c] Superconducting Materials Laboratory, Graduate School of Science and Engineering, Shibaura Institute of Technology 3-7-5 Toyosu, Koto-Ku, Tokyo, 135-8548, Japan
[d] Department of Physics, Low-Temperature Physics Lab, Indian Institute of Technology Madras, Chennai, 600036, India

ARTICLE INFO

ABSTRACT

Substitution of alkali earth metal ion of Sr^{2+}, in the Pb^{2+} site of $Pb(Mg_{1/3}Nb_{2/3})O_3$–$PbTiO_3$ is expected to induce functional modulations in the system. Doping of 4 at.% of Sr^{2+} in 0.68PMN-0.32PT was carried out to lower the transition temperature, and to investigate the intended ferroelectric and dielectric variations. Excellent relaxor property was observed in the doped sample without appreciable reduction in remnant polarization. Doping with Sr^{2+} led to a reduction in transition temperature from 165 °C to 117 °C. Doped sample exhibited remnant polarization $P_r = 16.2\,\mu C/cm^2$, Squareness factor (Rsq) = 1.05 and Relaxor exponent (γ) around 2. Modulation in the functional response was exhibited by the doped composition, having low transition temperature, and its prospect in electrocaloric applications was analyzed.

1. Introduction

Enhanced functional response exhibited by $(1-x)[Pb(Mg_{1/3}Nb_{2/3})O_3]$-$x[PbTiO_3]$ in the morphotropic phase boundary (MPB) has contributed to the utilization of the system for various applications like sensors, actuators, capacitors *etc*. [1]. Structural fluctuations and bimodal microstructure which are observed in the MPB compositions (x = 0.30 to 0.35) of PMN-PT are attributed to the improved properties exhibited by the system [2]. While compositions with 'x' below 0.13 have cubic symmetry and are piezoelectrically inactive, 'x' in the range of 0.13–0.30 is expected to exhibit rhombohedral crystal symmetry with high dielectric constant. PMN-PT composition in the morphotropic phase boundary shows structural fluctuations from rhombohedral to tetragonal through one or two intermediate phases of low symmetry like monoclinic, orthorhombic and/or triclinic, and have enhanced ferroelectric response. Improved relaxor and/or ferroelectric behavior exhibited by PMN-PT systems, make them useful for a variety of piezoelectric and electromechanical applications [3,4].

It has been reported that unusually high functional response at the paraelectric-ferroelectric phase transition; and the depolarization cooling exhibited by the ferroelectric materials, makes them suitable for electrocaloric applications [5,6]. Since ferroelectric remnant polarization is considered a powerful attribute of a ferroelectric system, a correlation of remnant polarization *vs* electrocaloric response exhibited by the system would be worth researching. However, most of the well known ferroelectric systems with better functional response have not been tested for the electrocaloric response, as a lower electrocaloric working temperature (below 100 °C or so) is quite favorable for practical applications. For example, the compositions in the morphotropic phase boundary of (1-x) PMN-x PT with properties suitable for electromechanical applications have not been tested for electrocaloric applications [7], as their transition temperature ($T_m \sim 160$ °C) is much above the working temperature for electrocaloric applications and is determined by the percentage of titanium content in it [2]. However, PMN-PT compositions with 'x' below 0.10 have been tested for electrocaloric studies and applications [7–10].

But, the reduction in the percentage of PT would distort the ferroelectric response exhibited by the system as well and it has been found that having a higher P_r and a lower T_m in the PMN-PT system is a hurdle. Even though PMN-PT compositions with 'x' below 0.15 would exhibit reduced transition temperature (T_m below 100 °C), but, the compositions would be at the verge of rhombohedral or cubic crystal

symmetry of the system with enhanced relaxor behavior, which warrants a slim ferroelectric loop with extremely low remnant polarization [11]. *ie.* composition having a better relaxor nature would be ideal for enhanced electrocaloric studies. So, even though the high electrocaloric effect is expected for compositions in the MPB [12,13], in order to have T_m in the range of 100 °C, rhombohedral or cubic PMN-PT compositions with lower titanium contents are studied [11]. For PMN-PT composition with x = 0.32, the expected value of T_m is around 165 °C [2]. It has been reported earlier that, the phase transition temperature can be brought down by substitution of less polarizable species like Sr^{2+} in the Pb^{2+} site of the PMN-PT perovskite structure, which would bring down the total strain energy of the domain walls and in turn the activation energy for domain wall motion. A reduction of 20 °C in transition temperature per 1 at.% Sr^{2+} doping of the composition is expected [14]. The present study aimed at realizing pyrochlore free, single-phase Sr^{2+} doped 0.68PMN-0.32PT without using excess lead in the precursor and having a reduced T_m without a reduction in ferroelectric response. A study on variation in ferroelectric and dielectric response exhibited by the doped composition from the parent composition due to 4 at.% Sr^{2+} doping is analyzed.

2. Material and methods

In the present study, we prepared two composites, *viz.*, 0.68PMN-0.32PT [undoped parent composition (S_A)] and doped with 4 at.% Sr^{2+} (S_B). Synthesis of S_A and S_B was performed through the columbite B-site precursor method [15]. Stoichiometric proportions of the precursors, $MgNb_2O_6$ (prepared by solid-state reaction route) [16], TiO_2 and PbO were mixed uniformly by thorough mechanical grinding for 2 h. Partial covering method and modulated stabilization heating were adopted to suppress the lead loss and to prevent pyrochlore formation. The stabilization of the synthesized ceramic was done at 1050 °C for 4 h during calcination to enable the completion of phase formation. Calcined single-phase ceramic powder samples were further ground, pressed and then sintered at 1150 °C for 4 h to realize dense ceramic pellets for property studies. A uni-axial pressure of 350 MPa was applied for making green pellets.

Crystallographic property of the powder sample was performed to confirm phase formation and the absence of the pyrochlore phase in the sintered pellets using X-ray diffraction (XRD) [Rigaku Smart Lab X-ray diffractometer, Japan] and Raman spectroscopy (Witec confocal Raman microscope) studies. The XRD data was recorded in the range of 2θ = 20° to 80°. Ar laser having wavelength 488 nm was used for excitation in Raman spectra analysis of the sintered pellets. Silver paint was applied on both sides of the bulk pellets and was heated to 600 °C with a dwell time of 10 min to have stable electrodes for electrical measurements. To study the relaxor response and shift in T_m dielectric measurements were carried out in the frequency range 1 Hz–100 kHz using Alpha High Resolution Dielectric/Impedance Analyzer (Novocontrol, Germany) using 1 V amplitude for probing AC electric signal in the temperature range 30 °C–250 °C (temperature increment was restricted to 5 °C around T_m). The data were recorded during cooling (cooling rate 1 °C/min) to prevent error due to degassing during heating. The ferroelectric studies (P-E hysteresis studies) were performed using Radiant PE loop tracer (Radiant Technologies, USA) by placing the unpoled disc into silicone oil. A sinusoidal signal with the driving frequency of 12 Hz was used for recording the hysteresis response. The density of the ceramic pellets was calculated using Archimedes' water displacement kit attached with Mettler Toledo sensitive balance using deionized water as the liquid medium. To correlate the functional response with microstructure and to understand the effect of Sr^{2+} dopant on the crystal symmetry, surface and cross-sectional morphology of the ceramic pellets were captured using scanning electron microscopy (JEOL 7100 FEG, Japan) and were analyzed. Also, to confirm uniform doping of Sr^{2+} in the bulk ceramic, energy dispersive spectroscopy (EDS) imaging on the broken pellets were done.
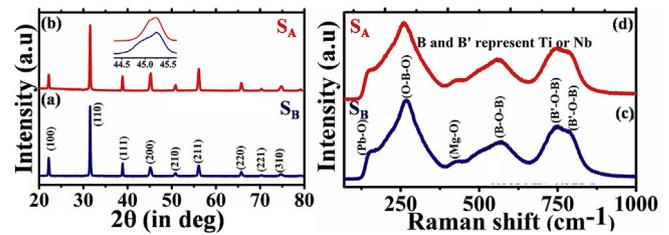

Fig. 1. Shows XRD (left) and Raman spectroscopy (right): (a) & (c) for sample S_B and (b) &(d) for S_A. Inset (left) shows magnified region (2θ = 44.5° to 45.5°).

3. Results and discussion

3.1. X-ray diffraction and Raman spectroscopy

Fig. 1 shows the X-ray diffractogram and Raman spectroscopy images of samples S_A ((b) and (d)) and S_B ((a) and (c)), respectively. X-ray diffractograms of both the compositions exhibit signature peaks of the PMN perovskite phase (Fig. 1) without any trace of the secondary pyrochlore phase. The absence of a secondary pyrochlore phase in the system can be attributed to the homogeneous distribution of elements, reduction of lead loss due to partial covering method and modulated heating adopted for ceramic synthesis [16]. Multiple diffraction peaks observed in the range 2θ = 44.5° to 45.5° is the signature of the morphotropic phase boundary and is an indication of the presence of mixed crystal symmetry in the system. Absence of any noticeable peak shift in Sr^{2+} doped samples, (note the peak position at 2θ = 45.236°) indicates that unit cell dimension is unaffected by doping and the same could be attributed to the identical valency (2^+) and the comparable ionic radius of Pb^{2+} and Sr^{2+}. Expected lattice distortion with Sr^{2+} doping was not detected in XRD as well as Raman spectroscopy which may be due to the extremely low concentration of dopants used in the study. Reduction in the splitting of the peak around 2θ = 45° observed in Sr^{2+} doped sample compared to parent composition may be attributed to the presence of tetragonal structure close to MPB [17]. While S_A exhibited the characteristic prominent structural co-existence of MPB, S_B showed twin peak around 2θ = 45°, which may be attributed to the formation of tetragonal crystal symmetry due to Sr^{2+} doping. Identical valency (2^+), coordination numbers (12), atomic radius (Pb-163 p.m. and Sr – 158 p.m.) and comparable ionic radii of Pb^{2+} and Sr^{2+} ensure the substitution of Sr^{2+} in the A-site (Pb-site) of PMN-PT [18,19]. No noticeable variation in Raman spectra was observed between the two samples. Observed Raman modes may be attributed to, *viz.*, 270 cm^{-1} to O - B – O, 450 cm^{-1} to Mg - O, 580 cm^{-1} to B - O – B and 790 cm^{-1} to B - O – B' (B and B' stand for Nb or Ti)). Raman spectrum also confirms the absence of a secondary phase in the parent composition as well as in the doped system [2,16].

3.2. Microstructure study

Significant variation in the cross-sectional and surface morphology of the doped composition as observed in Fig. 2b and 2c can be attributed to the sample's additional thermodynamic driving force available for decomposition and enhanced tetragonality with Sr^{2+} addition [20,21]. The pores observed in the surface morphology (shown in circles in panel (b)) must be due to the loss of PbO from the surface due to low vaporization temperature, or due to excess percentage of Sr^{2+}, which push out more Pb from the lattice site. Two types of grain boundaries are expected in the grain growth of PMN-PT based systems in the MPB which expect bimodal grain patterns [Fig. 2 (a)]. According to the grain boundary studies done by Rheinheimer and Hoffmann [22], a typical grain is characterized by misorientation, inclination, energy, and mobility. While the boundary having enhanced mobility favors the growth of coarse grains (bigger size grains), smaller size grains are correlated to low mobility boundary type [22] and hence the bimodal
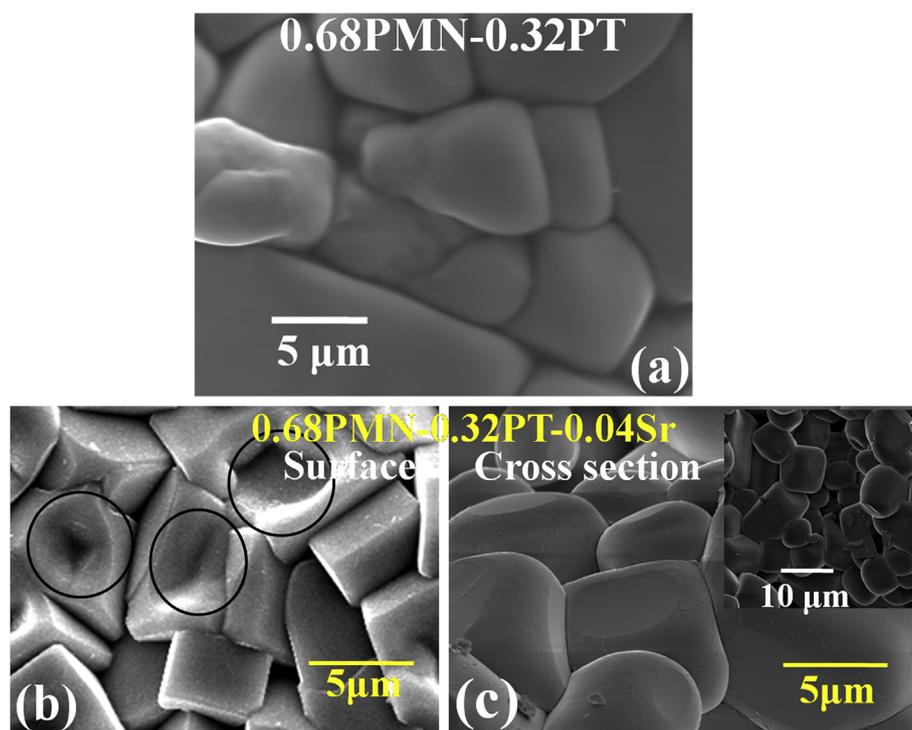
Fig. 2. SEM images: (a) undoped ceramic (S_A) pellet (b) surface image (circles in panel shows evaporation of the Pb species from the surface) and (c) bulk cross section of Strontium doped PMN-PT ceramic pellet (S_B).(inset of (c) represents SEM image recorded at lower magnification, which shows pores in the ceramic).

grains observed could be attributed to the increased growth rate of high mobility grain boundaries over low mobility ones. However, slowest boundaries would dominate during grain growth, as fast-growing grains are constrained by the slower grains which is the reason for the increased number of smaller sized grains seen in the microstructure shown inset, (which is taken with lower magnification) (Fig. 2 c) [23,24]. Increased grain growth observed in the microstructure images of S_B could be attributed to the presence of Sr^{2+} doping in the lattice sites [Fig. 2 (c)], which favors grain growth [11,25]. No surface decomposition was noticed in the undoped sample and sharp edges/grain boundaries were observed in the surface morphology [(Fig. 2(b)] compared to that in cross-section. The density of the sample S_A was found to be 7.68 g/cc while that of S_B was 7.58 g/cc [21]. The relative density of the doped composition was quite identical with the parent composition (~94% of the theoretical density for Sr^{2+} doped composition) and is ascribed to the intrinsic change in the ionic diffusivity brought about by the presence of Sr^{2+} ions in the lattice, which aids the densification process. The slight reduction in density observed in S_B may be attributed to the decline in the coupling between grains which arise due to PbO loss.

To confirm uniform doping of Sr^{2+} in the ceramic and the absence of pyrochlore secondary phase in the compositions, an elemental analysis was carried out through EDS mapping in the cross-section of the composites, which are shown in Figs. 3(a) and 4(a). The mapping profiles of the S_B sample displayed uniform distribution of Sr element in all the grains selected for scanning, which establish the uniform substitution of Sr^{2+} ions into the lattice of the crystal system. No trace of the secondary phase is seen in the EDS mapping in both undoped and doped ceramics. As the elemental mapping profile for component elements exhibited uniform and identical intensity distribution, the possibility of a secondary phase in the sample could be ruled out, which was confirmed earlier through XRD and Raman spectroscopy studies as well. Since Pb evaporation was observed in the surface morphology [Fig. 2(b)], an EDS line scan was carried out on the bulk microstructure which could not detect the presence Pb deposition along the grain boundary; and hence, ruled out the possibility of a reduction in

ferroelectric response due to conducting lead in the grain boundary. An increased count of elemental Pb on the surface of the composition was also not detected in the study [X-ray diffraction data [Figs. 3(b) and 4(b)].

3.3. Ferroelectric study

Variation in the ferroelectric response due to Sr^{2+} addition is evident from the hysteresis loop traced for S_B composition (Fig. 5). Comparison of ferroelectric response exhibited by the two compositions is given in Table 1. The reduction in the value of ferroelectric parameters *viz.* saturation polarization (P_{sat}), remnant polarization (P_r) and coercive electric field (E_C); exhibited by S_B compared to S_A is a vindication of the increase in relaxor characteristics developed in the composition. Since E_C is a measure of the energy barrier to the B-site cations, a decrease in E_C exhibited by S_B could be attributed to the lower jump barrier encountered by the B-site cations or smaller external field needed to switch the occupying sites [26]. For perfect relaxor ferroelectrics with polar nano regions, the squareness factor (R_{sq}) is expected to be close to 1.0 [16,27]. The values of R_{sq} obtained for the S_A and S_B compositions are 1.22 and 1.05 respectively, which suggests the enhanced relaxor nature of the Sr^{2+} doped composition. Reduction in the polarization ratio (P_r/P_{sat}) for doped samples (~0.73) compared to the undoped sample (~0.83), also confirms an improved relaxor response due to doping. Comparable ferroelectric response exhibited by S_A and S_B may be attributed to the compensating effect of the increase in the degree of tetragonality of the doped system [28], which favors ferroelectric behavior with augmented relaxor response in the system. Although a considerable increase in tetragonal symmetry should have facilitated an increase in ferroelectric response [20], it was not observed in this study. The same is confirmed from the bulk morphology which is of the bimodal type expected for morphotropic phase boundary compositions of PMN-PT. Reduction in ferroelectric response seen in the doped composition contrary to the expectation may possibly be attributed to the microstructural antagonistic effect which is indicated in Fig. 2(c) inset. Also, a higher breakdown field of 17 kV/cm is
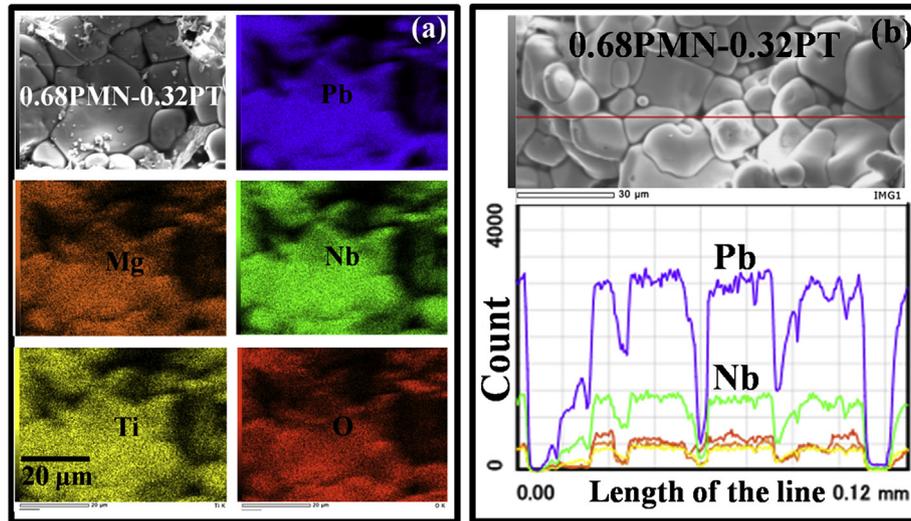
Fig. 3. Elemental analysis on sample S_A: (a) Mapping measurement and element profiles (b) line scan measurement along the grain boundaries.

favorable for enhanced variation in temperature with the application of an electric field (electrocaloric applications) [7].

Reduced absolute area (999) of the ferroelectric loop for doped composition is an indication of low ferroelectric loss under the application of the alternating electric field. Recoverable energy densities of the compositions are obtained by subtracting the calculated area from the total area and represent the available energy per unit volume of dielectric on discharge. Recoverable energy that can be obtained during the cycle of electrification is calculated and displayed in Fig. 5 (iii and iv). Recoverable energy is calculated using the origin software from the P-E response. The boundary between the two colors in Fig. 5(iii) and Fig. 5 (iv) is the upper portion of the hysteresis graph in the first quadrant, which touches on the Polarization axis at P_r and extends to saturation polarization. Area of the portions marked blue [Fig. 5 (iii)] and red [Fig. 5 (iv)] represents recoverable energy density which is calculated based on the details available elsewhere [2,29,30]. Though there is a slight reduction in recoverable energy noticed in S_B compared to S_A due to the enhanced relaxor nature of S_B, it is still quite reasonable for the utility of the ceramic for applications. Higher recoverable energy of the system may be attributed to the increased tetragonal symmetry of the doped composition against rhombohedral/cubic symmetry of (1-x) PMN-x PT systems [2]. Compositions tested for the electrocaloric response in PMN-PT, which was mentioned earlier ('x' below 0.15) were
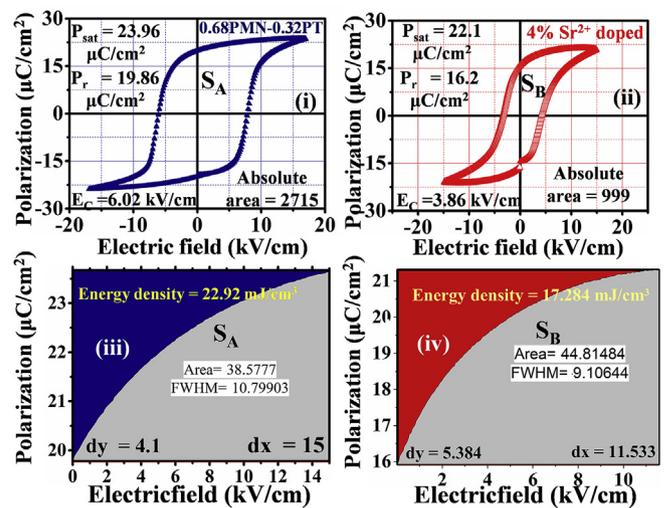

Fig. 5. (i) & (ii) show ferroelectric response (Polarization vs Electric field) and (iii) and (iv) show recoverable energy calculations. [Fig (i) and (iii) are of S_A & (ii) and (iv) that of S_B, respectively].
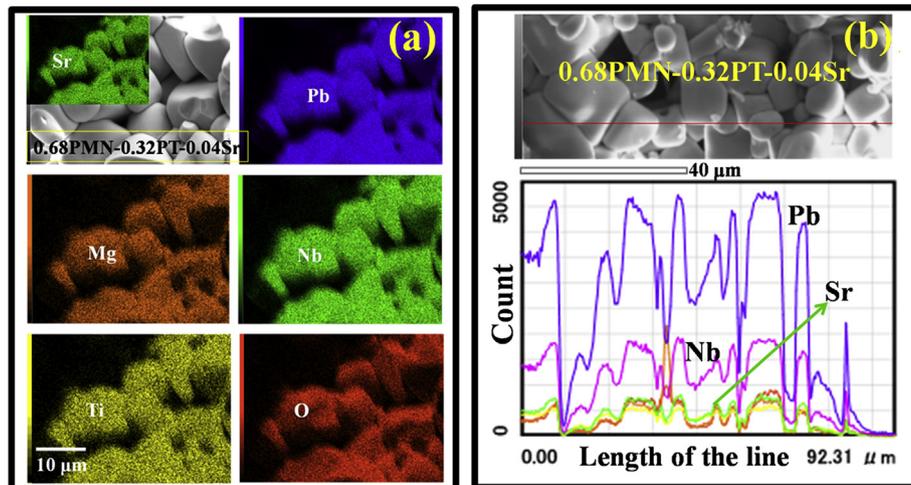

Fig. 4. EDS measurements on sample S_B: (a) Mapping profile (image corresponds to Sr^{2+} (inset) shows uniform distribution of the dopant (b) line scan (No traces of Pb deposition along the grain boundary were observed).

Table 1
Comparison of ferroelectric properties of 0.68PMN-0.32 PT (S_A) and 4 at. % Sr^{2+} doped compositions (S_B).

Attribute	S_A	S_B
P_{sat} ($\mu C/cm^2$)	23.96	22.1
P_r ($\mu C/cm^2$)	19.86	16.2
E_C (kV/cm)	6.02	3.86
Squareness (R_{sq})	1.22	1.05
Absolute area	2715	999
Range of E (kV/cm)	± 17	± 15
Recoverable energy density (mJ/cm^3)	22.92	17.28

systems having rhombohedral/cubic crystal symmetry. The appreciable energy density of the Sr^{2+} doped composition obtained in the study may be further explored to understand the suitability of the system for electrocaloric and other applications. Reduction in recoverable energy observed in S_B compared to the parent compound S_A is due to the increase in the relaxor response of Sr^{2+} doped system.

In the Positive up Negative down (PUND) test, a non-switching pulse was used after one pulse, in contrast to traditional P-E loop measurements where the applied voltage goes to a negative maximum after the applied positive maximum voltage. The signal trend (Fig. 6(a)) was also found to be different from the sinusoidal signal which is used in normal hysteresis measurements. These magnify the difference between true polarization and the polarization affected by several other factors (like leakage current *etc.*). The remnant field as observed in PUND test are: $+P^*_r = 27.65\,\mu C/cm^2$ and $-P^*_r = -28.23\,\mu C/cm^2$ while the $+dP_r$ and $-dP_r$ are $22.08\,\mu C/cm^2$ and $23.82\,\mu C/cm^2$, respectively.

3.4. Dielectric study

Variation in dielectric response with temperature and frequency for S_A ((i) and (iii)) and S_B ((ii) and (iv)) are shown in Fig. 7. Both exhibit frequency dispersion, which is characteristic of relaxor ferroelectric systems. The value of ferroelectric to the paraelectric phase transition is identified from the temperature corresponding to the peak value of dielectric permittivity (ε_r), which showed that the T_C of S_A and S_B was 164.5 °C and 117 °C, respectively. Reduction in ε_r and T_C of S_B could be attributed to lattice distortion and deformation of phase structure induced by the dopant in the lattice [31,32].

Although frequency dispersion was observed in both compositions, a shift in dielectric maximum towards higher temperature with frequency, expected in relaxor systems was not observed in our study. This
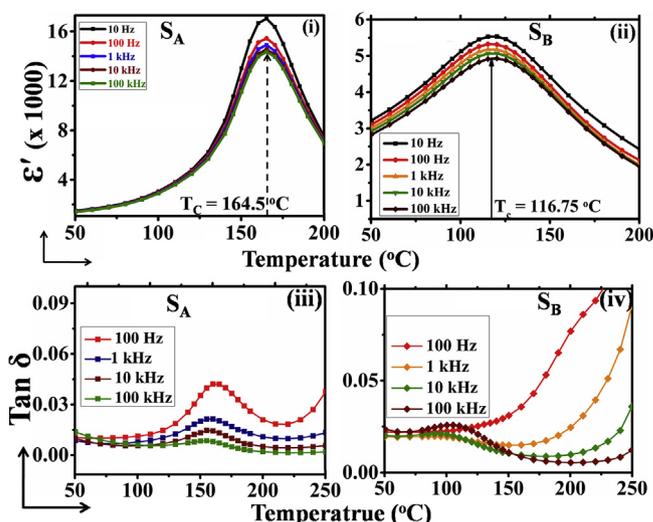

Fig. 7. (i) and (ii) shows variation of real part of dielectric permittivity (ε') with temperature, at different frequencies. (i) S_A and (ii) S_B. Shift in T_C (~165 °C for S_B to ~117 °C for S_B) & (iii) and (iv) shows variation in loss tangents with temperature, at various frequencies. (Tanδ values are shown only for higher frequencies).

confirms that Sr^{2+} doped composition is still in the MPB region as in basic composition with structural integration and enhanced degree of tetragonality in the system. A similar response was also reported earlier in PMN-PT composition in the morphotropic phase boundary [33]. However, ideal relaxor nature with frequency dispersion of dielectric permittivity and shift in T_m is generally expected for (1-x) PMN-x PT compositions with a lower value of 'x' (x = 0.15 and below), which are away from MPB. The reduction in the dielectric response may be attributed to the improved tetragonality setting in the composition due to the presence of Sr^{2+} dopants, as rhombohedral or cubic crystal symmetry is favorable for enhanced dielectric response [2]. This confirms that system S_B retains the morphotropic traits of undoped composition (S_A), as higher dielectric constant contrary to that expected for systems with low titanium content. Since the dielectric constant greatly depends on the grain size and domain structure [34–37], a decrease in the dielectric constant obtained in S_B may be due to the reduction in the percentage of coarse grains in the bimodal microstructure, which affects the dielectric response of the doped ceramic [38–40]. Reduction in the percentage of coarse grains results in an increase in the grain boundaries, which adversely affects dielectric permittivity. However, the maximum dielectric loss (Tanδ) in the vicinity of ferroelectric to paraelectric transition temperature is found to be less than 0.03 for both undoped and doped samples, which attests to the quality of the ceramics for dielectric and ferroelectric applications.

The absence of characteristic relaxor nature in S_B, in spite of reduced T_m, confirms that the doping of Sr^{2+} in MPB composition does not induce the characteristics of (1-x) PMN-x PT with the lower value of 'x' in the composition. This could be attributed to the presence of tetragonality of the crystal system as has been discussed earlier. (1-x) PMN-x PT compositions with 'x' below 0.15, which are generally used for electrocaloric studies, are expected to show higher dielectric response and reduced T_m due to the presence of rhombohedral crystal symmetry. The broadening of the dielectric dispersion observed in the doped composition may be attributed to the heterogeneity in domain structures present in the system due to the addition of Sr^{2+}, which in turn cause a distribution of T_m within the ceramics [14]. The broadening of the dielectric permittivity seen with Sr^{2+} doping was earlier reported in Sr^{2+} doped PZT, which showed a larger distribution of Curie temperature [41,42]. Considerable increase in the diffuse phase transition (DPT) behavior of doped composition seen in Fig. 3(ii) is confirmed with the analysis of the value of the relaxor exponent [Fig. 7
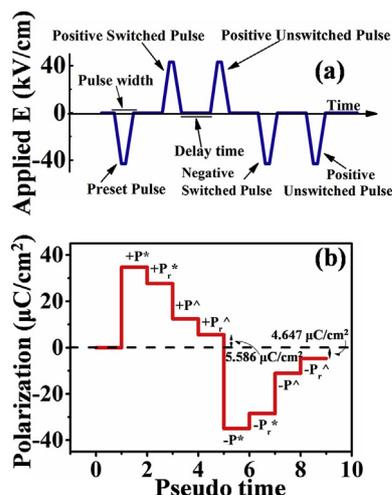

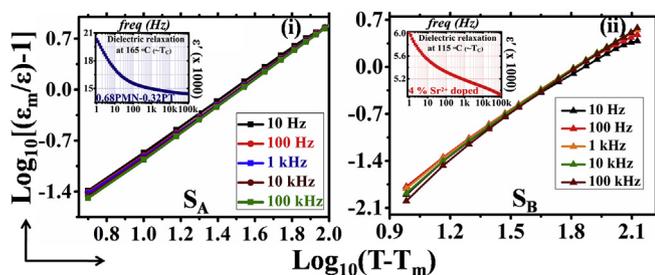**Fig. 6.** (a) Applied electrical pulse for measuremnt- PUND response and (b) PUND response for S_B sample.

Fig. 8. Variation of $\log_{10}[(\varepsilon_m/\varepsilon)-1]$ vs $\log_{10}(T-T_m)$ for various frequencies (i) S_A and (ii) S_B. Dielectric relaxations exhibited at Tc are shown inset.

Table 2
Dielectric analysis and relaxation response exhibited by S_A and S_B, in the range 100 Hz to 100 kHz.

Frequency	ε_{max}		$Tan\delta_{max}$		γ	
	S_A	S_B	S_A	S_B	S_A	S_B
100 Hz	15501	5324	0.042	0.024	1.76	1.95
1 kHz	14969	5179	0.020	0.018	1.79	1.98
10 kHz	14623	5066	0.015	0.021	1.81	2.01
100 kHz	14411	4929	0.007	0.026	1.83	2.02

and Table 2].

Dielectric analysis of PMN-PT like relaxor system, in MPB with an enhanced degree of tetragonality, is done using Lorentz type relaxation behavior [33,43]. Linear fitting was done to calculate the relaxor exponent of S_A and S_B samples which is displayed in Fig. 8 (i) and (ii) respectively. Relaxor nature exhibited by the compositions is also depicted in the inset. Variation of the real part of dielectric permittivity and loss tangent with temperature and frequency exhibited by the samples were analyzed (Fig. 8). Dielectric response of the relaxor material can be analyzed using a modified Curie-Weiss law, which is given below.

$$(1/\varepsilon) - (1/\varepsilon_m) = [(T-T_m)^\gamma]/C \quad (1)$$

Where ε_m is the maximum value of dielectric permittivity at the transition temperature (T_m), C is the Curie-like constant and γ is the value of relaxor factor or Curie-Weiss exponent, which will exhibit value in the range from 1 to 2. The slope of $\log_{10}[(\varepsilon_m/\varepsilon)-1]$ vs $\log_{10}(T-T_m)$ plot is a measure of relaxor exponent, (Fig. 8), the value of which gives the extent of dielectric relaxation expected of the system. The value of $\gamma = 1$ corresponds to the sharp phase transition expected in the normal ferroelectric system, whereas $\gamma = 2$ corresponds to a perfect relaxor ferroelectric system with a clean diffuse phase-transition (DPT) behavior [33,44]. A comparison of the dielectric response of the two samples is given in Table 2. The slope of linear fitting on the logarithmic function of the equation will give the value of the relaxor exponent, which is compared in Table 2. The relaxor exponent value ($\gamma > 1.7$) confirms a diffuse type first order ferroelectric-paraelectric phase transition [45]. Relaxor exponent is increased in S_B compared to S_A, which could be attributed to the rise in the relaxor characteristic of the system. Both, squareness factor and relaxor exponent obtained for Sr^{2+} doped composition support the shift in the composition towards relaxor side.

Though an appreciable increase in relaxor nature with Sr^{2+} doping was outlined, no appreciable variation in characteristic relaxor behavior (shift in temperature corresponding to the dielectric maximum with frequency) which is expected of (1-x) PMN-x PT with lower 'x' value was observed. Nearly constant temperature for dielectric maximum corresponding to various frequencies is evident from Fig. 7(ii). This could be due to an enhanced degree of tetragonality in the doped system. An increase in the value of relaxor exponent noticed may be

attributed to lattice distortion induced by the dopant, which hinders the long-range dipole alignment or enhances in the polar nano regions (PNR) within the system [46]. Also, the disruption of dipolar coupling in the system by Sr^{2+} diminishes the correlation length and favors the reduction in domain size or formation of more PNR regions [47,48].

4. Conclusion

The pyrochlore-free 0.68PMN-0.32 PT composite is synthesized and the effect of 4 at.%
Sr^{2+} doping is investigated. XRD and Raman spectroscopy confirmed the absence of secondary and paraelectric pyrochlore phase. Dielectric and ferroelectric modulations due to the doping of Sr^{2+} were investigated and correlated with the structure and microstructural analysis carried out on the composites. Sr^{2+} doping caused an increase in relaxor behavior and a reduction in T_m (165 °C to 117 °C) without an appreciable reduction in remnant polarization. Low ferroelectric loss due to reduced absolute area (999), higher recoverable energy density (17.284 mJ/cm^3), a higher value of P_r (16.2 μC/cm^2) and low T_m obtained in the Sr^{2+} doped composition, favors ferroelectric applications. Enhanced relaxor response was confirmed through parameters such as squareness factor ($R_{sq} = 1.05$), $E_C = 3.86$ kV/cm relaxor exponent $\gamma \sim 2$. The diffuse phase transition along with lower value of transition temperature (~117 °C) obtained without loss in remnant polarization, is favorable for electrocaloric applications.

Declaration of competing interest

The authors declare that they have no known competing financial interests or personal relationships that could have appeared to influence the work reported in this paper.

References

[1] K.Y. Zhao, W. Ruan, H.R. Zeng, J.T. Zeng, G.R. Li, Q.R. Yin, Domain dynamics of La-doped PMN-PT transparent ceramics studied by piezoresponse force microscope, Appl. Surf. Sci. 293 (2014) 366–370.

[2] P. Augustine, M. Rath, M.S. Ramachandra Rao, Enhanced functional response of high temperature stabilized (1-x) PMN-x PT ceramics, Ceram. Int. 43 (2017) 9408–9415.

[3] S.W. Choi, R. TR Shrout, S.J. Jang, A.S. Bhalla, Dielectric and pyroelectric properties in the Pb (Mg$_{1/3}$Nb$_{2/3}$)O$_3$-PbTiO$_3$ system, Ferroelectrics 100 (1) (1989) 29–38.

[4] A.S. Mischenko, Q. Zhang, R.W. Whatmore, J.F. Scott, N.D. Mathur, Giant electrocaloric effect in the thin film relaxor ferroelectric 0.9 PbMg$_{1/3}$Nb$_{2/3}$O$_3$–0.1 PbTiO$_3$ near room temperature, Appl. Phys. Lett. 89 (24) (2006) 242912 (1-3).

[5] D.Q. Xiao, Y.C. Wang, R.L. Zhang, S.Q. Peng, J.G. Zhu, B. Yang, Electrocaloric Properties of (1−x) Pb (Mg$_{1/3}$Nb$_{2/3}$)O$_3$–xPbTiO$_3$ ferroelectric ceramics near room temperature, Mater. Chem. Phys. 57 (2) (1998) 182–185.

[6] T.M. Correia, J.S. Young, R.W. Whatmore, J.F. Scott, D. MathurN, Q. Zhang, Investigation of the electrocaloric effect in a PbMg$_{2/3}$Nb$_{1/3}$O$_3$–PbTiO$_3$relaxor thin film, Appl. Phys. Lett. 95 (1–3) (2009) 182904.

[7] Lovro Fulanović, SilvoDrnovšek, Hana Uršič, Marko Vrabelj, KostjaMakarovič DanjelaKuščer, Vid Bobnar, ZdravkoKutnjak, Barbara Malič, Multilayer 0.9 Pb (Mg$_{1/3}$Nb$_{2/3}$) O$_3$–0.1PbTiO$_3$ elements for electrocaloric cooling, J. Eur. Ceram. Soc. 37 (2) (2017) 599–603.

[8] J. Peräntie, H.N. Tailor, J. Hagberg, H. Jantunen, Z.-G. Ye, Electrocaloric properties in relaxor ferroelectric (1 −x) Pb(Mg$_{1/3}$Nb$_{2/3}$)O$_3$–xPbTiO$_3$system, J. Appl. Phys.

(1–6) (2013) 174105 114.

[9] L. Shaobo, L. Yanqiu, Research on the electrocaloric effect of PMN/PTsolid solution for ferroelectrics MEMS micro cooler, Mater. Sci. Eng. B 113 (4) (2004) 6–9.

[10] S. Hirose, T. Usui, S. Crossley, B. Nair, A. Ando, X. Moya, N.D. Mathur, Progress on electrocaloric multilayer ceramic capacitor development, Apl. Mater. 4 (1–6) (2016) 064105.

[11] C. Molin, M. Sanlialp, V.V. Shvartsman, D.C. Lupascu, P. Neumeister, A. Schönecker, S. Gebhardt, Effect of dopants on the electrocaloric effect of 0.92Pb (Mg$_{1/3}$Nb$_{2/3}$) O$_3$–0.08 PbTiO$_3$ ceramics, J. Eur. Ceram. Soc. 35 (7) (2015) 2065–2071.

[12] D. Saranya, A.R. Chaudhuri, J. Parui, S.B. Krupanidhi, Electrocaloriceffectof PMN–PT thin films near morphotropic phase boundary, Bull. Mater. Sci. 32 (2) (2009) 59–62.

[13] R. Chukka, J.W. Cheah, Z. Chen, P. Yang, S. Shannigrahi, J. Wang, L. Chen, Enhanced cooling capacities of ferroelectric materials at morphotropicphase boundaries, Appl. Phys. Lett. 98 (1–3) (2011) 242902.

[14] Hong Zheng, et al., Effects of octahedral tilting on the piezoelectric properties of strontium/barium/niobium-doped soft lead ZirconateTitanate ceramics, J. Am. Ceram. Soc. 85 (9) (2002) 2337–2344.

[15] S.L. Swartz, T.R. Shrout, Fabrication of perovskite lead magnesium niobate, Mater. Res. Bull. 17 (1982) 1245–1250.

[16] P. Augustine, M.S. Ramachandra Rao, Realization of device quality PMN–PT ceramics using modulated heating method, Ceram. Int. 41 (2015) 11984–11991.

[17] H. Zheng, I.M. Reaney, W.E. Lee, N. Jones, H. Thomas, Effects of octahedral tilting on the piezoelectric properties of strontium/barium/niobium-doped soft lead ZirconateTitanate ceramics, J. Am. Ceram. Soc. 85 (9) (2002) 2337–2344.

[18] R.D. Shannon, Revised effective ionic radii and systematic studies of interatomic distances in halides and chalcogenides, Acta Crystallogr. A 32 (1976) 751–767, https://doi.org/10.1107/S0567739476001551 number 5.

[19] Y. Wang, Z. Gui, Y.C. Chan, L. Li, X. Zhang, Effect of dopants on aging properties for the PMN–0.1 PT relaxor ferroelectric ceramics, J. Mater. Sci.: Mater. Electron. 13 (1996) 3–5 7.

[20] H. Zheng, I.M. Reaney, W.E. Lee, N. Jones, H. Thomas, Surface decomposition of strontium-doped soft PbZrO$_3$–PbTiO$_3$, J. Am. Ceram. Soc. 85 (1) (2002) 207–212.

[21] M.S. Silva, R.G. Dias, E.F. Souza, M. Cilense, M.A. Zaghete, A.A. Cavalheiro, Effect of strontium doping on the structural, morphological, and dielectric properties of PZT ceramics, Mater. Sci. Forum 869 (2016) 8–12 (Trans Tech Publications).

[22] W. Rheinheimer, M.J. Hoffmann, Grain growth in perovskites: what is the impact of boundary transitions? Curr. Opin. Solid State Mater. Sci. 20 (5) (2016) 286–298.

[23] M. Bäurer, M. Syha, D. Weygand, Combined experimental and numerical study on the effective grain growth dynamics in highly anisotropic systems: application to barium titanate, Acta Mater. 61 (15) (2013) 5664–5673.

[24] M. Upmanyu, G.N. Hassold, A. Kazaryan, E.A. Holm, Y. Wang, B. Patton, D.J. Srolovitz, Boundary mobility, and energy anisotropy effects on microstructural evolution during grain growth, Interface Sci. 10 (2002) 201–216.

[25] Volkan Kalem, Ibrahim Cam, MuharremTimuçin, Dielectric and piezoelectric properties of PZT ceramics doped with strontium and lanthanum, Ceram. Int. 37 (4) (2011) 1265–1275.

[26] J.C. Ho, K.S. Liu, I.N. Lin, Study of ferroelectricity in the PMN-PT system near the morphotropic phase boundary, J. Mater. Sci. 28 (1993) 4497–4502.

[27] R. Cao, G. Li, J. Zeng, S. Zhao, L. Zheng, Q. Yin, The piezoelectric and dielectric properties of 0.3Pb(Ni$_{1/3}$Nb$_{2/3}$)O$_3$–xPbTiO$_3$–(0.7-x)PbZrO$_3$ ferroelectric ceramics near the morphotropic phase boundary, J. Am. Ceram. Soc. 93 (3) (2010) 737–741.

[28] H. Zheng, I.M. Reaney, W.E. Lee, N. Jones, H. Thomas, Effects of strontium substitution in Nb-doped PZT ceramics, J. Eur. Ceram. Soc. 21 (13) (2001) 71–75.

[29] X. Zhao, Z. Zhou, R. Liang, F. Liu, X. Dong, High-energy storage performance in lead-free (1-x) BaTiO3-xBi (Zn0.5Ti0.5)O3 relaxor ceramics for temperature

stability applications, Ceram. Int. 43 (2017) 9060–9066.

[30] S. Samanta, V. Sankaranarayanan, K. Sethupathi, Effect of Nb and Fe co-doping on microstructure, dielectric response,ferroelectricity and energy storage density of PLZT, J. Mater. Sci. Mater. Electron. 29 (2018) 20383–20394.

[31] D. Maurya, H.C. Song, M.G. Kang, Processing, Properties, and Design of Advanced Ceramics and Composites: Ceramic Transactions vol. 259, Wiley, Daytona Beach, 2016, pp. 99–115.

[32] N. Zhong, W.L. Yao, P.H. Xiang, S. Kojima, Calcium substituting B-site in relaxor ferroelectrics with perovskite structure probed by chemical ordering, Solid State Commun. 134 (6) (2005) 425–429.

[33] A. Slodczyk, P. Daniel, A. Kania, Local phenomena of (1 − x)PbMg$_{1/3}$Nb$_{2/3}$O$_3$-xPbTiO$_3$ single crystals (0 ≤ x ≤ 0.38) studied by Raman scattering, Phys. Rev. B. 77 (1–16) (2008) 184114.

[34] N. Setter, L.E. Cross, The role of B-site cation disorder in diffuse phase transition behavior of perovskite ferroelectrics, J. Appl. Phys. 51 (8) (1980) 4356–4436.

[35] B.P. Pokharel, R. Ranjan, D. Pandey, V. Siruguri, S.K. Paranjpe, Rhombohedral superlattice structure and relaxor ferroelectric behavior of (Pb$_{0.70}$Ba$_{0.30}$)ZrO$_3$ ceramics, Appl. Phys. Lett. 74 (5) (1999) 756–758.

[36] K.M. Lee, H.M. Jang, A New mechanism of nonstoichiometric 1: 1 short-range ordering in NiO-doped Pb(Mg$_{1/3}$Nb$_{2/3}$)O$_3$Relaxor ferroelectrics, J. Am. Ceram. Soc. 81 (10) (1998) 2586–2596.

[37] J. Chen, A. Gorton, H.M. Chan, M.P. Harmer, Effect of powder purity and second phases on the dielectric properties of lead magnesium niobate ceramics, J. Am. Ceram. Soc. 69 (12) (1986) C-303-305.

[38] X. Zhao, W. Qu, H. He, N. Vittayakorn, X. Tan, Influence of cation order on the electric field-induced phase transition in Pb(Mg$_{1/3}$Nb$_{2/3}$)O$_3$-based relaxor ferroelectrics, J. Am. Ceram. Soc. 89 (1) (2006) 202–209.

[39] M. Promsawat, J.Y.Y. Wong, Z. Ren, H.N. Tailor, A. Watcharapasorn, Z.G. Ye, S. Jiansirisomboon, Enhancement in dielectric, ferroelectric, and electrostrictive properties of Pb (Mg$_{1/3}$Nb$_{2/3}$)0.9Ti$_{0.1}$O$_3$ ceramics by CuO addition, J. Alloy. Comp. 587 (2014) 618–624.

[40] R. Yao, Y. Liu, C. Lyu, N. Xu, Z. Yu, Y. Lyu, Impact of Ni dopant on the structure and electrical properties of PMN-0.1 PT ceramics, J. Mater. Sci. Mater. Electron. (2017) 1–7.

[41] H. Zheng, I.M. Reaney, W.E. Lee, N. Jones, H. Thomas, Effects of strontium substitution in Nb-doped PZT ceramics, J. Eur. Ceram. Soc. 21 (10) (2001) 1371–1375.

[42] M. Khalid, M. Shoaib, A.A. Khan, Strontium doped lead zirconate titanate ceramics: the study of calcination and sintering process to improve the piezo effect, J. Nanosci. Nanotechnol. 11 (6) (2011) 5440–5445.

[43] K. Uchino, S. Nomura, Critical exponents of the dielectric constants in diffused-phase-transition crystals, Ferroelectrics 44 (1) (1982) 55–61.

[44] S. Ke, H. Fan, H. Huang, H.L.W. Chan, Lorentz-type relationship of the temperature-dependent dielectric permittivity in ferroelectrics with diffuse phase transition, Appl. Phys. Lett. 93 (4–7) (2008) 112906.

[45] Z. Xia, L. Wang, W. Yan, Q. Li, Y. Zhang, Comparative investigation of structure and dielectric properties of Pb (Mg$_{1/3}$Nb$_{2/3}$)O$_3$–PbTiO$_3$ (65/35) and 10% PbZrO$_3$-doped Pb (Mg$_{1/3}$Nb$_{2/3}$)O$_3$–PbTiO$_3$ (65/35) ceramics prepared by a modified precursor method, Mat. Res. Bull. 42 (2007) 1715–1722.

[46] J. Wu, Y. Chang, B. Yang, X. Wang, S. Zhang, Y. Sun, X. Qi, J. Wang, W. Cao, Densification behavior and electrical properties of CuO-doped Pb (In$_{1/2}$Nb$_{1/2}$) O$_3$–Pb(Mg$_{1/3}$Nb$_{2/3}$)O$_3$–PbTiO$_3$ ternary ceramics, Ceram. Int. 42 (6) (2016) 7223–7229.

[47] N. Zhong, P.H. Xiang, D.Z. Sun, X.L. Dong, Effect of rare earth additives on the microstructure and dielectric properties of 0.67Pb(Mg$_{1/3}$Nb$_{2/3}$)O$_3$–0.33PbTiO$_3$ ceramics, Mater. Sci. Eng., B 116 (2) (2005) 140–145.

[48] X.H. Dai, Z. Xu, D. Viehland, Correlation of freezing dynamics and the domain-like states in relaxor ferroelectrics, Ferroelectrics 176 (1996) 91–97.